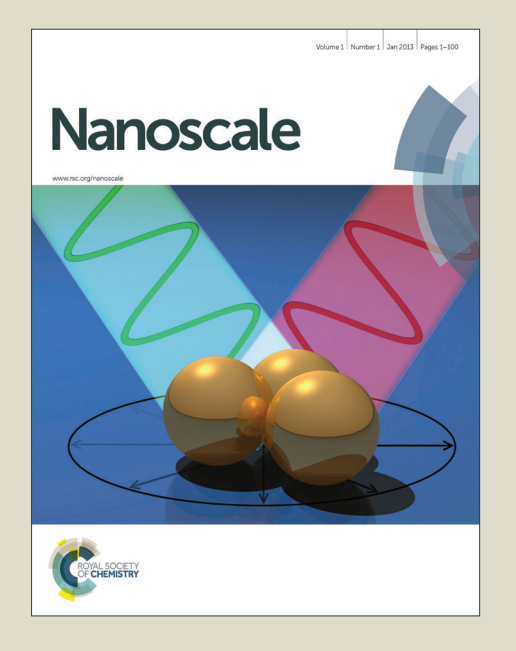
Nanoscale

Accepted Manuscript



This is an *Accepted Manuscript*, which has been through the Royal Society of Chemistry peer review process and has been accepted for publication.

Accepted Manuscripts are published online shortly after acceptance, before technical editing, formatting and proof reading. Using this free service, authors can make their results available to the community, in citable form, before we publish the edited article. We will replace this Accepted Manuscript with the edited and formatted Advance Article as soon as it is available.

You can find more information about *Accepted Manuscripts* in the **Information for Authors**.

Please note that technical editing may introduce minor changes to the text and/or graphics, which may alter content. The journal's standard <u>Terms & Conditions</u> and the <u>Ethical guidelines</u> still apply. In no event shall the Royal Society of Chemistry be held responsible for any errors or omissions in this *Accepted Manuscript* or any consequences arising from the use of any information it contains.



Spin density wave in periodically strained Graphene Nanoribbon

Nabil M. Al-Aqtash^{a,b*} and Renat .F. Sabirianov^{a,b}

^aDepartment of Physics, University of Nebraska at Omaha, Omaha, Nebraska 68182-0266,USA

^b Nebraska Center for Materials and Nanoscience, University of Nebraska, Lincoln, Nebraska 68588-0111, USA

Abstract

Zigzag graphene nanoribbons (ZGNRs) are antiferromagnetic in the ground state with zero net magnetization due to the compensation of contributions from opposite edges. The uniform deformations (both shear and axial) do not produce magnetization due to the symmetry restrictions. However, we report the results of first-principles calculations that predict that the induction of spin density wave (SDW) in ZGNR under non-uniform periodic strain. Using density functional theory (DFT) method, we show that a sinusoidal magnetization variation along the axis of the ribbon occurs under a sinusoidal transversal shear strain. SDW appears due to the presence of strain gradient that induced asymmetry of magnetization on opposite edges of ZGNR which do not compensate each other. The amplitude of SDW is estimated at $\sim 0.066 \mu_B$ when deformations transverse to ZGNR axis have a sinusoidal profile with period of 88.6Å and amplitude of 1Å. Our study suggests that the periodic lattice deformations strongly affect the magnetic structure of ZGNRs in case of acoustic phonon or mechanical wave.

^{*}Corresponding author. Tel: +1 4025543727. E-mail address: nalaqtash@unomaha.edu (N. Al-aqtash)

1- Introduction

Properties of graphene, the strongest and most flexible as well as stretchable material can be tuned by mechanical deformations.¹ In principle, by suitable engineering of local strain profiles, all-graphene electronics could be integrated on a single graphene sheet. In other words, the combination of in-plane stiffness and off-plane flexibility of graphene is extraordinary, and the future applications of its mechanical effects will be valuable.

Several mechanical deformations of graphene and graphene nanoribbon (GNR), such as roughening, bending, folding, buckling, and twisting, are controllably produced in laboratories, ^{2,3,4,5} Periodic deformation occurs in case of phonon excitations or mechanical waves (intrinsic ripples). These excitations are expected in the graphene-based electronic and spintronics devices. 6 Mechanical deformations naturally appear in ZGNR. For example, AFM images of the chemically derived ZGNRs deposited on substrate show substantial bending when nanoribbons are less than 20nm wide. 7 Young et al. by using Raman spectroscopy have shown that the distribution of strain across the graphene monolayer is relatively uniform at levels of applied strain up to 0.6% but that it becomes highly nonuniform above this strain. 8 Moreover, there were reports of controlled texturing on graphene nanoribbons and membrains. Bao et al. reported the first direct observation and controlled creation of one- and two-dimensional periodic ripples in suspended graphene sheets, using both spontaneously and thermally generated strains. Yu et al. demonstrated atomic control of strain in freestanding graphene using a local attractive force created at the STM tip. 10 Moreover, mechanical vibrations in suspended nanoribbon were generated by D. Garcia-Sanchez et al. with sinusoidal variation of strains. 11

The magnetism of graphene has attracted considerable interest. An increase in the difference between the number of removed A and B sites of the graphene bipartite lattice at zig-

zag edges induces net magnetic moments and yields to ferromagnetism, particularly in nano-size graphene flakes and nanopores.¹² Recently, a clear hysteresis in magnetization reversal curves of ferromagnetic (FM) zig-zag edged graphene was reported.¹³ The magnetism is mainly was proposed in modified graphene sheet and in GNR where magnetism comes on the zig-zag termination of the graphene sheet.¹⁴ The ground state of zig-zag terminated GNR (ZGNR) is antiferromagnetic (AFM). There were several proposals to stabilize the ferromagnetic (FM) state in ZGNR by external factors, such as an interface with magnetic materials^{14,15}, an application of an external magnetic field¹⁶ or an electric field¹⁷.

Long spin diffusion length (>2 µm at room temperature) offers an exceptional basis for development of spintronic devices. ¹⁸ Proximity effects were predicted in graphene by magnetic insulators, such as EuO, point toward the possible engineering of spin gating. ¹⁹ Spin-filtering at interfaces between close-packed surfaces of Ni or Co and graphite or graphene were predicted with ideal spin-injection. ²⁰ However, only a moderate (~10%) magnetoresistance (MR) was observed at room temperature in a spin valve where graphene is sandwiched by two FeNi electrodes. ²¹ Recently, a nearly 100% negative MR was observed at low temperatures, and maintained MR=56% at room temperature. ²² In addition, several theoretical studies have suggested that GNRs could exhibit magneto-electronic properties, with a very large predicted MR. ^{4,23,24}

Although, the study of magnetic properties and mechanical properties in graphene systems were investigated in great details, the mutual effect of mechanical deformations and magnetic properties has not been extensively addressed.

In this study, based on density functional theory (DFT) calculations, we show that a spin density wave is induced in sinusoidally shear-strained ZGNRs. These types of deformations

occur in case of phonon excitations as well as in case of propagation of mechanical waves. Specifically, this deformation corresponds to a transverse acoustic phonon mode in infinite graphene sheet with in-plane atomic displacements.

2- Model and Computational Method

We consider N-ZGNR (N zigzag chains in width) as a periodic supercell consisting 36 primitive unit cells of total length $L=88.6\text{\AA}$, where N=4.5, ...12. The modeling of a sinusoidal strain deformation in nanoribbon is performed by sinusoidal transverse displacement $u_v = A\sin(2\pi x/L)$, where x = 0..L is the x-axis atomic positions, L = 88.6Å is the nanoribbon length. The y-coordinate of an atom in the strained ribbon is calculated as $v_i = v_{i0} + u_v$, where v_{i0} is yposition of atom in unstrained ZGNR, Amplitude A is varied from 0 to 5Å. Figure 1 shows a schematic atomistic model of sinusoidally shear-strained 4-ZGNR. Although the model does not describe actual phonon excitations in ZGNR, it captures the origin of spin-lattice interactions. Specifically, it allows direct investigation of the effect of flexure (curvature) on the magnetism of ZGNR. To study the effects of the edge symmetry and width of N-ZGNR, we use the 5-, 7-, 9-, 11-ZGNRs and the 4-,6-, 8-, 10-, 12-ZGNRs to represent asymmetric ZGNRs and symmetric ZGNRs, respectively. Moreover, to investigate the effect of period (L) of the sinusoidal strain, we considered 4-ZGNR of three period sizes: L= 88.6Å (supercell consisting of 36 primitive unit cells), 59.07 Å (supercell consisting of 24 primitive unit cells), and 44.3Å (supercell consisting of 18 primitive unit cells).

Our computational approach is based on an *ab initio* pseudopotential method in the framework of density functional theory. ^{25,26} The geometry relaxations and electronic structures of the nanoribbons are calculated by using SIESTA package,²⁷ using numerical atomic orbitals as basis sets and Troullier-Martin type ²⁸ norm-conserving pseudopotentials. Local Spin Density

Approximation (LSDA) is used with the exchange-correlation functional in Ceperley-Alder (CA) form.²⁹ The self-consistent calculations are performed with a 350Ry mesh cutoff. A linear combination of numerical atomic orbitals with double- ξ polarizations (DZP) basis set is used. The convergence criteria for energy were selected to be 10^{-5} eV. The conjugate gradient method is used to relax the ionic coordinates until the force on each atom is less than 0.01 eV/Å.

3- Results and Discussion

We started by performing electronic and ionic relaxation for the planar N-ZGNRs with antiferromagnetic spin configuration to obtain the ground state structures. Then, the nanoribbons were strained by applying a sinusoidally varying shear strains (described by its amplitude A). This deformation corresponds to a transverse acoustic phonon mode in infinite graphene sheet with in-plane atomic displacements. Our system models a frozen phonon with $k=2\pi/L$. This mode is higher in energy than the ZA acoustic phonon with out-of-plane displacements. However, if out-of plane displacements are suppressed this may become the lowest energy phonon excitation. We performed self-consistent electronic structure calculations for the strained nanoribbons while keeping the atomic positions frozen. Figure 2-(a) shows calculated magnetization induced locally, M, in 4-ZGNRs as a function of the amplitude A at L=88.6, 59.07 and 44.3Å. We find that symmetry between magnetic moment at opposite sides of ZGNR is lifted and magnetization is induced locally along the nanoribbon. The induced magnetization is calculated as a total magnetic moment for half-period of strained ZGNR with the same sign of the in-plane curvature. The induced magnetization increases nearly linearly with the increase of the strain amplitude A of the ribbon until it reaches a saturation value. At higher values of A the induced magnetization is approximately constant. The strain amplitude at which the saturation is reached depends on the period of applied strain L. For

L=88.6Å the saturation occurs at A=3Å, while the saturation is reached at A=2Å for ZGNR of L=44.3Å. The value of the induced magnetization at saturation increases as function of period L. This is expected because the induced magnetization depends on the number of edge atoms in the half period. Additionally, the same amplitude of sinusoidal deformation creates larger strain gradient in ZGNR with shorter period of deformation. We plot in Figure 2-(b) the induced magnetization, M, per edge atom as function of the strain gradient amplitudes, i.e. A multiplied by k-vector (kA). M(kA) for ZGNR of different period of deformation collapse into one curve. Clearly, the magnetization per edge atom scales nicely as function of strain gradient. Thus, the origin of induced magnetization is due to the presence of strain gradient.

Figure 3 shows the induced magnetization as functions of the width of strained asymmetric and symmetric ZGNRs for half (one arc) of the 88.6Å period with amplitude A=1Å. At the low values of nanoribbon width (N=4 to 6), we find dependence of edge magnetization on ZGNR thickness. When the width of the ZGNR changes form N=4 to 6 the value of the induced magnetization decreases from about 0.775 μ_B to 0.635 μ_B . However, with increase of the width the edge magnetization of the ribbon very quickly saturates, as we can see from the value of the induced magnetization for widths N=6 to 12. In term of the edge symmetry dependent, there are minor differences between the values of induced magnetization of asymmetric ZGNRs and symmetric ZGNRs, but they are not striking.

The magnetization induced in the ZGNR is due to the change in the local magnetic moments (LMMs) as function of the edge curvature. LMMs increase at the convex edge (with the positive curvature) and decrease at the concave edge (negative curvature). Figure 4 shows the LMMs of carbon atoms along half (one arc) of the 88.6\AA period of strained ZGNR with $A=1\text{\AA}$.

Strikingly the LMM dispersed in space just like a spin density wave with overall modulation similar to one of the frozen phonon displacements in real space. Thus, we observe the induction of the spin density wave by phonon-like deformation.

Figure 5 shows the variation of local magnetic moments along the edges of sinusoidally strained ZGNR with L= 88.6Å as well as magnetization as function of the positions of the carbon atom along the edge of 4-ZGNR x-axis. The latter is calculated as the sum of the local magnetic moments on opposite edges. Clearly there is correlation between mechanical deformations and the induced in spin density wave (SDW), with nodes of spin density wave occurring when opposite edges have the same zero local curvature. Here, we define the spin density wave (SDW) as a periodic modulation of electron spin density where period of modulation is different from the one of the ions in the ideal lattice. The maximum of SDW occur at positions with the largest difference in curvature of opposite edges. The fitting of SDW to the *sin* function shows nearly perfect match. Thus, SDW has the same spatial characteristic as the underlying deformation causing its appearance. The amplitude of SDW estimated at $\sim 0.066\mu_B$ for sinusoidal deformation (of amplitude A=1Å). This SDW amplitude is 1/3 of the local magnetic moments at the ZGNR edges ($\sim 0.2\mu_B$). Thus, spin-lattice coupling in graphene is very strong.

Typically, the spin-phonon coupling is relatively weak, but we find that in graphene this coupling is significant. This result is valid in Born-Oppenheimer approximation (ABO) because the frozen phonon-like deformation was used to model this coupling assuming that electronic structure adjusts fast compared to slow phonon movements. The validity of ABO in application to graphene has been discussed recently and our result could give an alternative way to explore this issue. ³⁰

Sinusoidal strain causes very small charge transfer at the edge atoms (less than

0.005*e*/site calculated per atomic sphere). Surprisingly, there is almost no charge transfer for sites of largest curvature. Thus, charge transfer is unlikely cause of SDW.

The origin of the induced SDW comes from the response of the local magnetic moments at two edges of ZGNR to the strain, specifically, non-uniform one. Although formally the inplane shear stress is the same at opposite edges of ZGNR, due to the termination, the edge stress is quite different at two opposing edges due to the curvature of edges. We introduce the area covered by radial from a carbon edge atom to two nearest carbon atoms as a measure of the local strain. We defined this area as the edge area "Area", which is calculated as:

$$Area = \frac{1}{2}\vec{r_1} \times \vec{r_2}$$

where r_1 , r_2 are vectors connecting the carbon atom at the edge to its nearest neighbors, as shown in Figure 6. Because this area is connected to the bond angle in carbon edge "chain", the increase/decrease of the edge area measures local deformations including not only bond length change but also the concavity. The connection between the shear strain and "Area" parameter is shown in Figure 6. The shear strain is defined as $\Delta u_y/a$, where $\Delta u_y = u_y(x + \Delta x) - u_y(x)$ is a deformation along y-axis occurring between two points separated by Δx , and a=2.42Å is a lattice constant of graphene unit cell. Clearly, the edges of opposite concavity have opposite trends with the increase of shear strain. i.e. this parameter is instrumental in distinguishing edges of different curvature.

In Figure 7 we superimposed the LMM variation as function of "area" parameter. The spin-density follows the sinusoidal distortions with the periodic modulations of local magnetic moments. To clarify the origin of spin-lattice interactions we studied the response of ZGNR to uniform deformations, i.e. tensile/compressive strains along the axis of the ribbon. We find that the uniform tensile strain causes the magnetization of the edge increase nearly linearly with

tensile strain, while compressive strain results in its near linear decrease as shown in Figure 6.

Clearly, there is overall correlation between results of uniform and non-uniform strain. However, this correspondence is far from being very close. There is obviously different slopes of M(A) for deformations at the opposite edges in case of sinusoidal deformations. Also, there is noticeable non-linearity of M(A). When amplitude of sinusoidal distortions increases, the deviations from the dependence between LMMs and area become strongly nonlinear.

There is a drastic difference in the effect made by distortions on the electronic states in ZGNR in case of uniform and non-uniform strains. The band structure in case of uniform compressive and tensile strains shows change in the dispersion of bands as shown in Figure 8. As we can see from the figure, the bands become more dispersed under compressive strain. Particularly, the energy of bands close to Fermi energy (E_F) at X point are not changing significantly under uniform strain while at Γ point the eigenvalues move further away, i.e. gets lower below E_F and higher above E_F . However, in addition to change in dispersion, bands of ZGNR with sinusoidal non-uniform strain shows an appearance of localized states which manifest itself as flat bands across the Brillouin zone separated on the energy scale from dispersed bands. Figure 9 shows a clear representation of this effect in E_K for 4-ZGNR at L=88.6Å and A=1Å.

The magnetization of unstrained ZGNR is zero due to the antiferromagnetic coupling of the opposite edges. The presence of the sinusoidal strain in ZGNR does not change total magnetization due to its symmetry. However, locally we may induce an asymetry between opposite edges due to the difference in its curvatures that results in local magnetic moment. The origin of this moment induction is due to the difference in the shift of electron states that appear upon non-uniform strain at opposite edges. To illustrate it we plot local densities of states

(LDOSs) for atoms at the edges of curvatures with opposite sign and compare them to atoms of near zero curvature, as shown in Figure 10(a and b) for 4-ZGNR with L=88.6Å. LDOSs were broadened by Gaussian with half-width σ =0.2 in SIESTA calculations to smooth out the sharp peaks of LDOSs due to the localized states. The figure shows that the atoms C_1 and C_2 that are located at the point of near zero curvature (although having a large shear strain) do not have strong asymmetry in LDOSs (Figure 10 a) and give near zero magnetic moment between two of them. Contrary, the atoms C_3 at the concave curvature point and C_4 at the convex curvature point have strong asymmetry in LDOSs with the main peak in majority LDOS for C_4 laying at lower energy than the one of C_3 LDOS (Figure 10 b). It causes the difference in occupation of states and resulting appearance of uncompensated local magnetic moment because C_4 has larger occupancy in majority LDOS than C_3 .

Figure 10(b-d) also illustrates the variation of LDOS of C3 and C4 atoms as function of magitude of strain amplitude, in case of 4-ZGNR with L=88.6Å. In unstrained (or uniformly strained) ZGNR the highest occupied bands have equal share of states from each edge site, i.e. each edge site has the same spin moment. However, with the increase of the amplitude of sinusoidal deformation, the contribution of the state at C3 to these bands decreases, while LDOS of C4 atom increases. At the amplitude A=3Å the LDOS of C3 atom at the highest occupied bands is very small and cannot reduce substantially with the further increase of the amplitude of deformation as can be seen in Figures 10c and 10d. At the same time LDOS of C4 also saturates at A=3Å (compare Figures 10c and 10d). Thus, the magnetization induced by the sinusoidal deformations is saturating at A=3Å and does not increase substantially with the further increase of A as can be seen in Figure 2.

The discussed above edge asymmetry can be used to induce a local magnetic moment in

graphene nanoribbons by inducing a curvature as we observe in sinusoidally strained ZGNR. Periodically strained edges may naturally appear in graphene nanoribbons without hydrogen termination.⁴ Particularly, mechanical vibrations in suspended nanoribbon may generate a standing wave in graphene nanoribbons with sinusoidal variation of strains.¹¹ The local moment can be measured by local probe methods such as sensitive magnetic force microscopy or spin-polarized scanning tunneling microscopy. The coupling between spin (magnon) and lattice (phonon) excitations can also be potentially observed in measurements of respected quasi-particle dispersions.

4- Conclusions

We show that sinusoidal strain deformations induce a spin-density wave along the axis of ZGNR with induced local magnetic moments modulating sinusoidally as well. While, the uniform deformations of ZGNR (both shear and axial) do not produce magnetization due to the symmetry restrictions, the deformations with gradient of strain (curvature) result in the local breaking of the symmetry and induction of local magnetization. SDW is induced due to the presence of strain gradient, the induced magnetization on opposite edges are not compensating each other. We estimate an amplitude of SDW of $\sim 0.066\mu_B$ that produced from the bending of ZGNR with the sinusoidal profile $\delta u_y = Asin(2\pi x/L)$ with A=1Å and L=88.6Å. Our study suggests that magnetic structure in ZGNR can be controllably modified using strain engineering.

References

- F. Guinea, M. I. Katsnelson and A. K. Geim, Nature Physics, 2010, 6, 30-33.
- J. C. Meyer, A. K. Geim, M. I. Katsnelson, K. S. Novoselov, T. J. Booth and S. Roth, Nature, 2007, 446, 60-63.
- 3 Z. H. Ni, T. Yu, Y. H. Lu, Y. Y. Wang, Y. P. Feng and Z. X. Shen, ACS Nano, 2008, 2, 2301-2305.
- T. W. Chamberlain, J. Biskupek, G. A. Rance, A. Chuvilin, T. J. Alexander, E. Bichoutskaia, U. Kaiser and A. N. Khlobystov, ACS Nano, 2012, 6, 3943–3953.
- 5 L. Elías, A. R. Botello-Méndez, D. Meneses-Rodríguez, V. J. González, D. Ramírez- González, L. Ci, E. Muñoz-Sandoval, P. M. Ajayan, H. Terrones and M. Terrones, Nano Lett., 2010,10, 366-372.
- 6 Y. Zhang, V. W. Brar, F. Wang, C. Girit, Y. Yayon, M. Panlasigui, A. Zettl and M. F. Crommie, Nature Physics, 2008, 4, 627-630.
- 7 X. Li, X. Wang, L. Zhang, S. Lee and H. Dai, Science, 2008, 319, 1229-1232.
- 8 R. J. Young , L. Gong , I. A. Kinloch , I. Riaz , R. Jalil and K. S. Novoselov, . ACS Nano, 2011, 5, 3079-3084.)
- 9 W. Bao, F. Miao, Z. Chen, H. Zhang, W. Jang, C. Dames and C. N. Lau, Nature Nanotechnology, 2009, 4, 562-566.)
- P. Xu, Y. Yang, S. D. Barber, M. L. Ackerman, J. K. Schoelz, D. Qi, I. A. Kornev, L. Dong, L. Bellaiche, S. Barraza-Lopez and P. M. Thibado, Phys. Rev. B, 2012, 85, 121406-121410(R).-
- D. Garcia-Sanchez, A. M. van der Zande, A. San Paulo, B. Lassagne, P. L. McEuen and A. Bachtold, Nano Lett., 2008, 8,1399–1403.
- 12 E. H. Lieb, Phys. Rev. Lett., 1989, 62, 1201-1204.
- 13 K. Tada, J. Haruyama, H. X. Yang, M. Chshiev, T. Matsui and H. Fukuyama, Phys. Rev. Lett., 2011, 107, 217203-217206.
- 14 M. Fujita, K. Wakabayashi, K. Nakada and K. Kusakabe, J. Phys. Soc. Jpn., 1996, 65, 1920-1923.
- 15 Y. Cho, Y. C. Choi and K. S. Kim, J. Phys. Chem. C, 2011, 115, 6019–6023.
- 16 W. Y. Kim and K. S. Kim, Nature Nanotech., 2008, 3, 408-412.

- 17 Y-W. Son, M. L. Cohen and S. G. Louie, Nature, 2006, 444, 347-349.
- N. Tombros, C. Jozsa, M. Popinciuc, H. T. Jonkman and B. J. van Wees, Nature (London), 2007;448, 571-574.
- 19 H. X. Yang, A. Hallal, D. Terrade, X. Waintal, S. Roche, and M. Chshiev, Phys. Rev. Lett., 2013, 110, 046603-046607.
- V. M. Karpan, P. A. Khomyakov, A. A. Starikov, G. Giovannetti, M. Zwierzycki, M. Talanana, G. Brocks, J. van den Brink and P. J. Kelly, Phys. Rev. B, 2008, 78, 195419-195429.
- 21 E. W. Hill, A. K. Geim, K. Novoselov, F. Schedin and P. Blake, IEEE. T. Magn., 2006, 42, 2694-2696.
- J. Bai, R. Cheng, F. Xiu, L. Liao, M. Wang, A. Shailos, K. L. Wang, Y. Huang and X. Duan, Nat. Nanotechnol., 2010, 5, 655-659.
- 23 F. Munoz-Rojas, J. Fernandez-Rossier and J. J. Palacios, Phys. Rev. Lett., 2009, 102, 136810-136813.
- 24 N. Al-Aqtash, H. Li, L. Wang, W. N. Mei and R. F. Sabirianov, Carbon, 2013, 51, 102-109.
- 25 P. Hohenberg and W. Kohn, Phys. Rev., 1964, 136, B864-B871.
- 26 W. Kohn and L. J. Sham, Phys. Rev., 1965, 140, A1133-A1138.
- J. M. Soler, E. Artacho, J. D. Gale, A. Garcia, J. Junquera, P. Ordejon and D. Sánchez-Portal, J. Phys.: Condens. Matter, 2002, 14, 2745-2779.
- N. Troullier and J. L. Martins, Solid State Commun., 1990, 74, 613-616.
- 29 J. P. Perdew, A. Zunger, Phys. Rev. B, 1981, 23, 5048–5079.
- 30 S. Pisana, M. Lazzeri, C. Casiraghi, K. S. Novoselov, A. K. Geim, A. C. Ferrari and F. Mauri, Nature Materials, 2007, 6, 198-201.

List of figure captions

Figure 1. Atomistic model for zig-zag graphene nanoribbon (4-ZGNR) with length L under sinusoidal deformation.

Figure 2. (a) Induced magnetization, M, defined as total magnetic moment on the half of the period of shear deformation, i.e. x=0..L/2 in Figure 1, as a function of amplitude of shear deformations (A) for three periods of deformation L (88.6, 59.07 and 44.3Å). (b) Induced magnetization, M, per edge atom as function of the strain gradient amplitudes, i.e. A multiplied by k-vector (kA).

Figure 3. Induced magnetization as functions of the width (N) of strained asymmetric and symmetric ZGNRs for half (one arc) of the 88.6 Å period with amplitude A=1Å.

Figure 4. Local magnetic moments as function of the x-position of the carbon atom along the edge of 4-ZGNR for the undeformed nanoribbon and the one sinusoidally strained with L=88.6 \mathring{A} and $A=1\mathring{A}$.

Figure 5. (Top panel) Local magnetic moments (LMMs) along the edges of sinusoidally strained 4-ZGNR. (Bottom panel) Spin density wave along the axis of ZGNR.

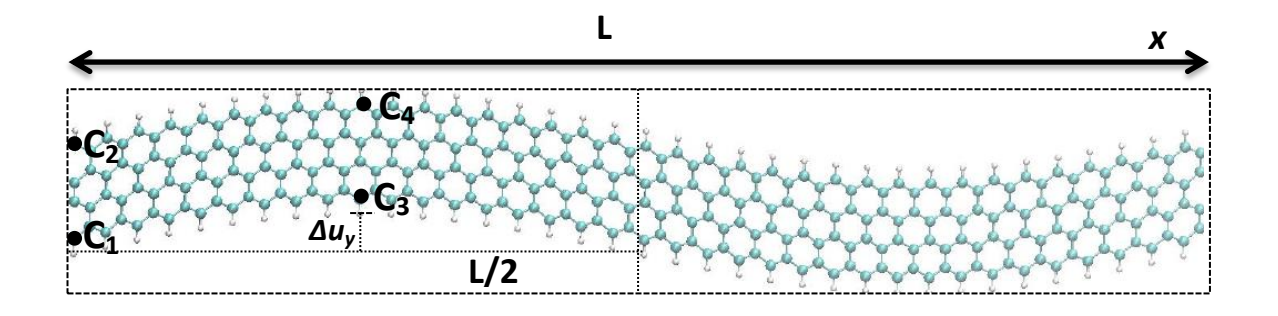
Figure 6. The edge area "Area" of sinusoidally strained (circles: convex edge, triangles: concave edge) 4-ZGNR as function of shear strain $(\Delta u_y/a)$.

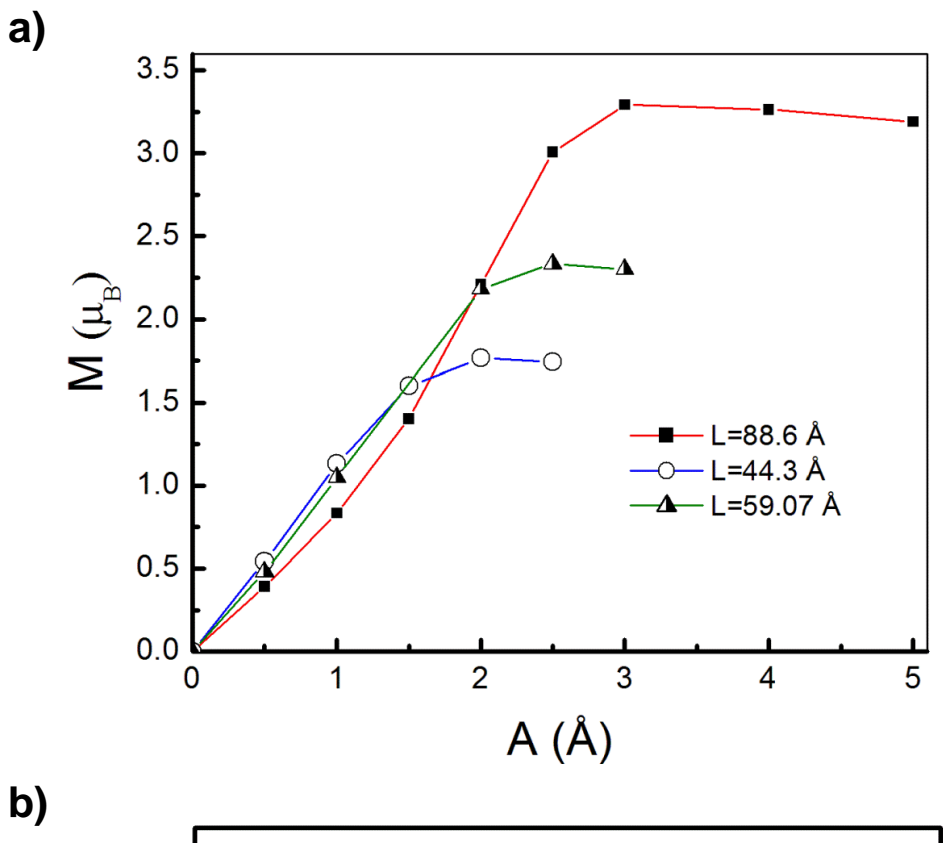
Figure 7. Local magnetic moments (LMMs) as function of the edge area of uniformly (black squares) and sinusoidally strained (circles: convex edge, triangles: concave edge) 4-ZGNR with $L=88.6 \, \text{Å}$. Main graph is for amplitude $A=1 \, \text{Å}$, insert is for $A=3 \, \text{Å}$.

Figure 8. The band structure of 4-ZGNR under compressive (1%) (upper panel) and tensile (1%) (lower panel) shown in red (xxx) compared to band structure of unstrained ZGNR shown in black (++++).

Figure 9. The band structure of 4-ZGNR with sinusoidal strain at A=1Å (upper panel) compared to band structure of unstrained 4-ZGNR (lower panel) at L = 88.6 Å.

Figure 10. Local densities of states (LDOSs) calculated for atoms of smallest local curvature (a) and the largest local curvature (b-d) for 4-ZGNR with sinusoidal strain at A=1, 3, 4 Å at L=88.6 Å. Notations of atoms follow Figure 1.





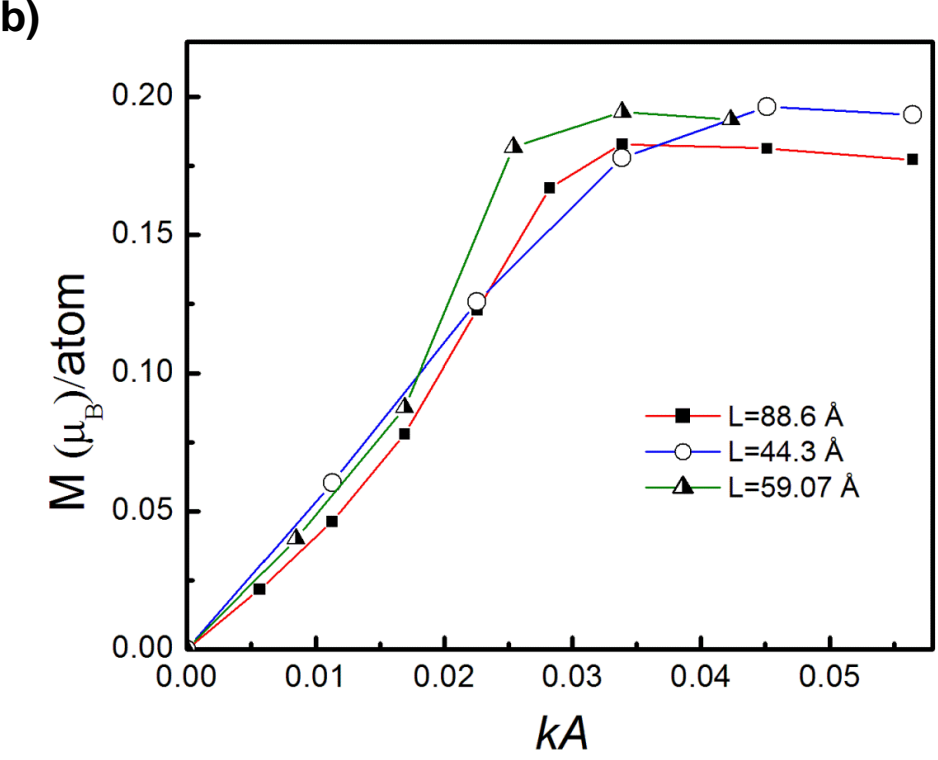
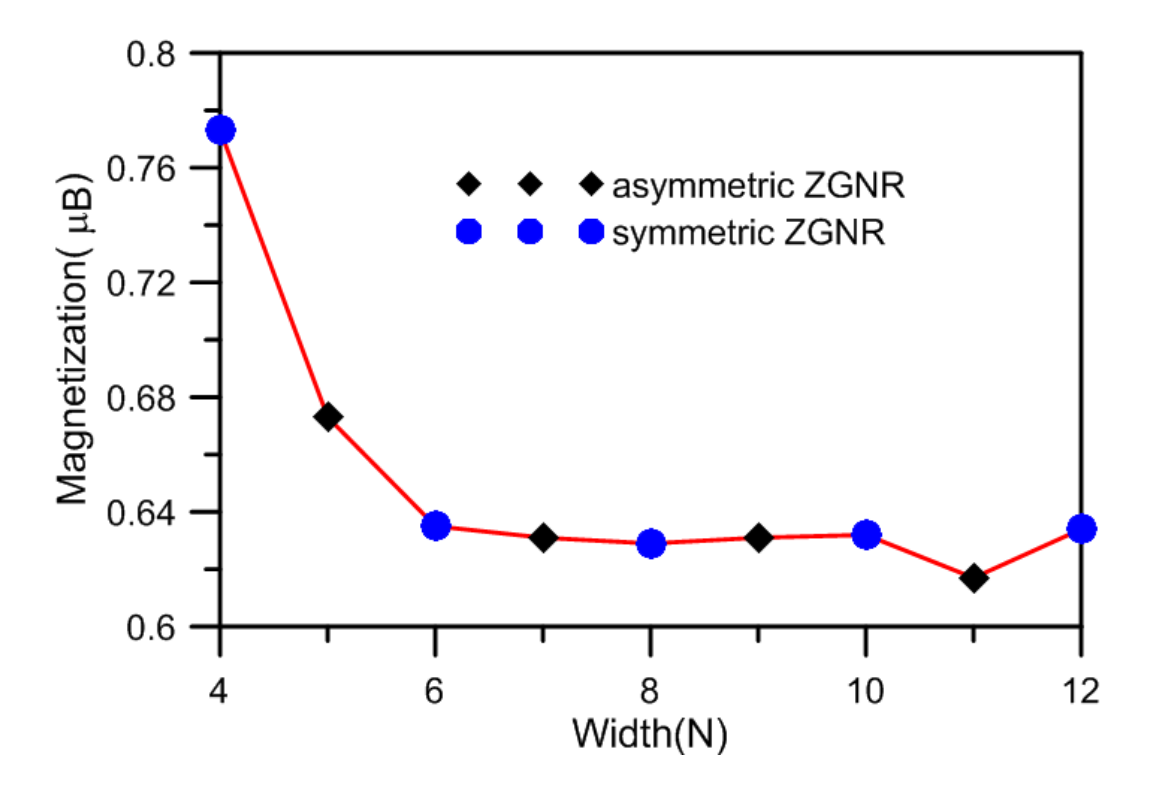
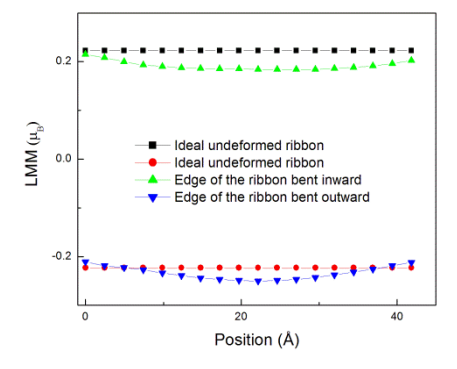
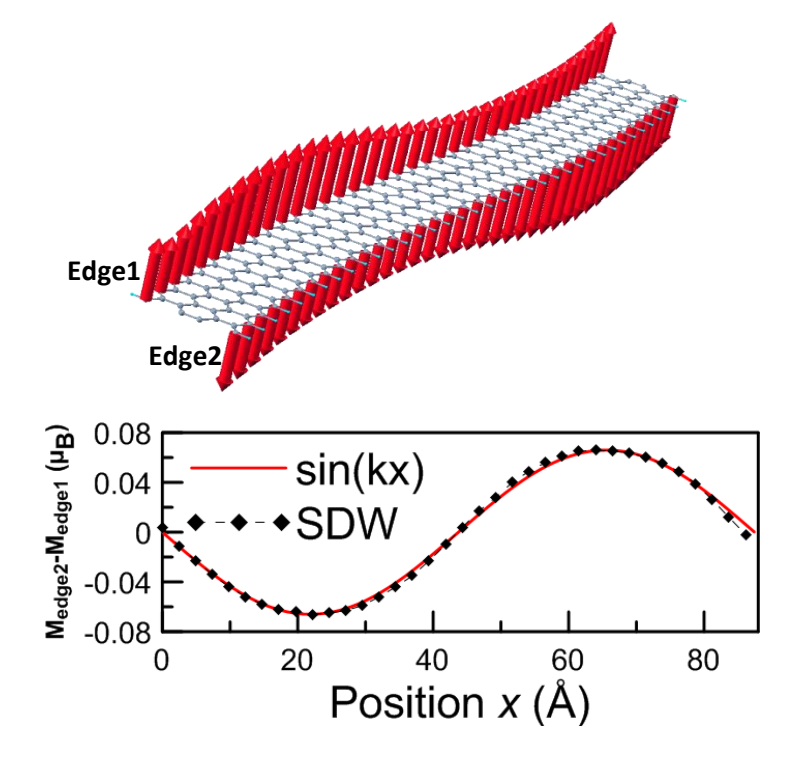


Figure 2







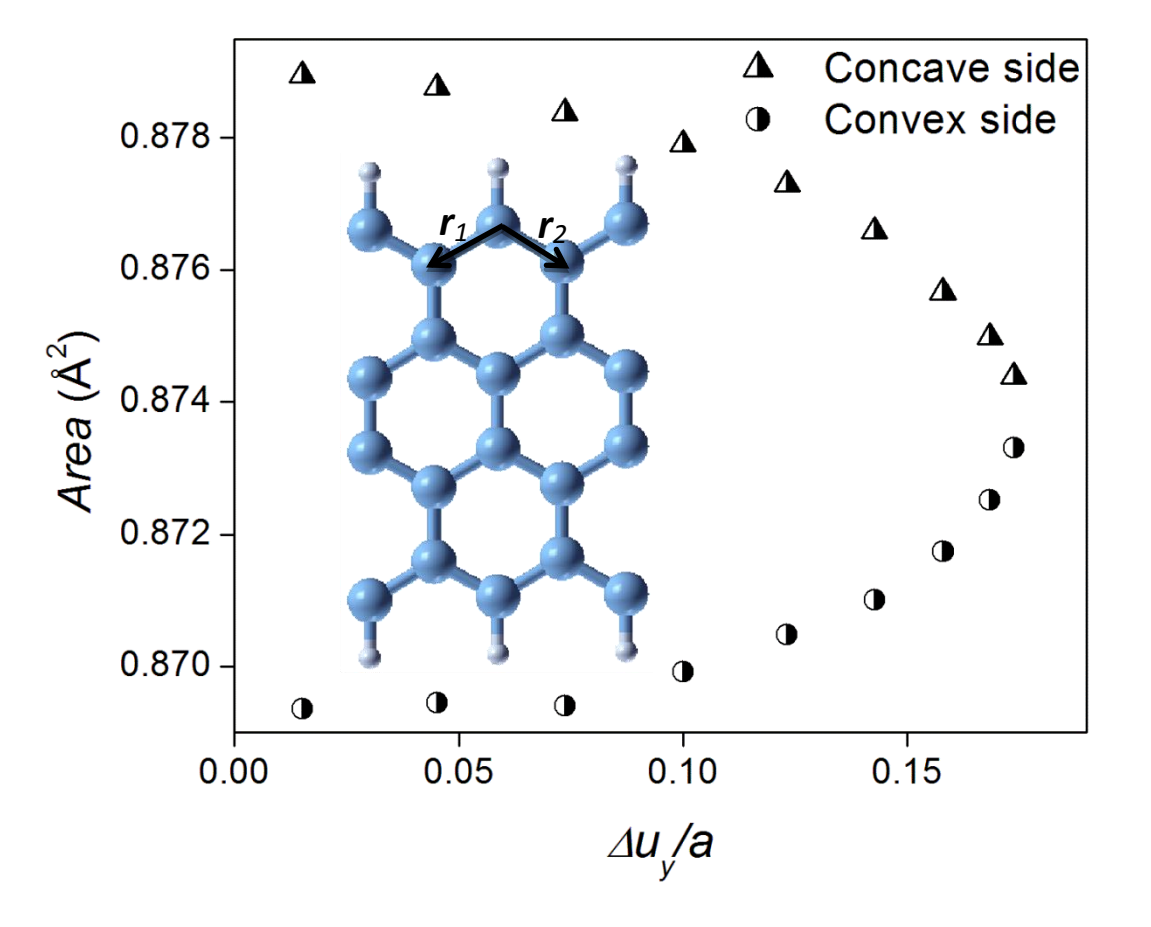
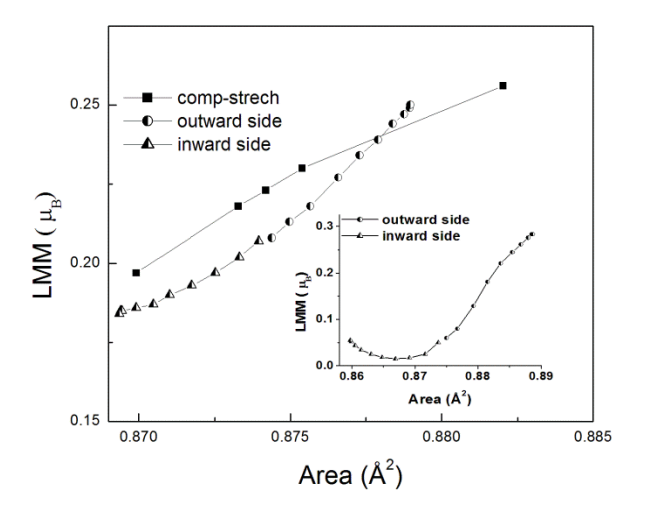


Figure 6



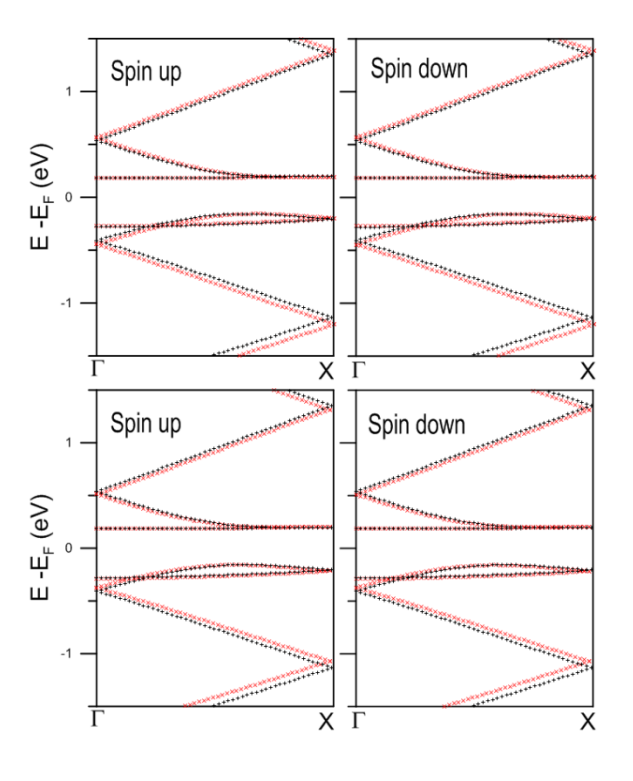
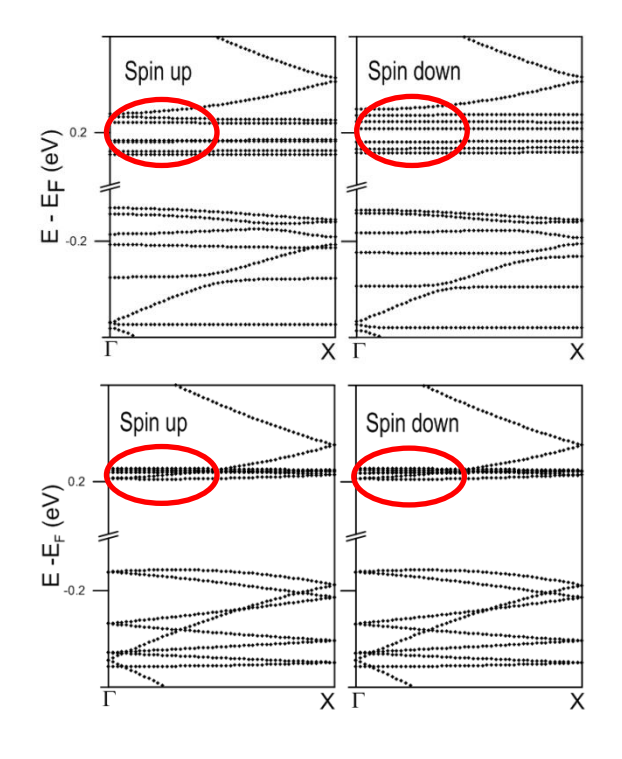


Figure 8



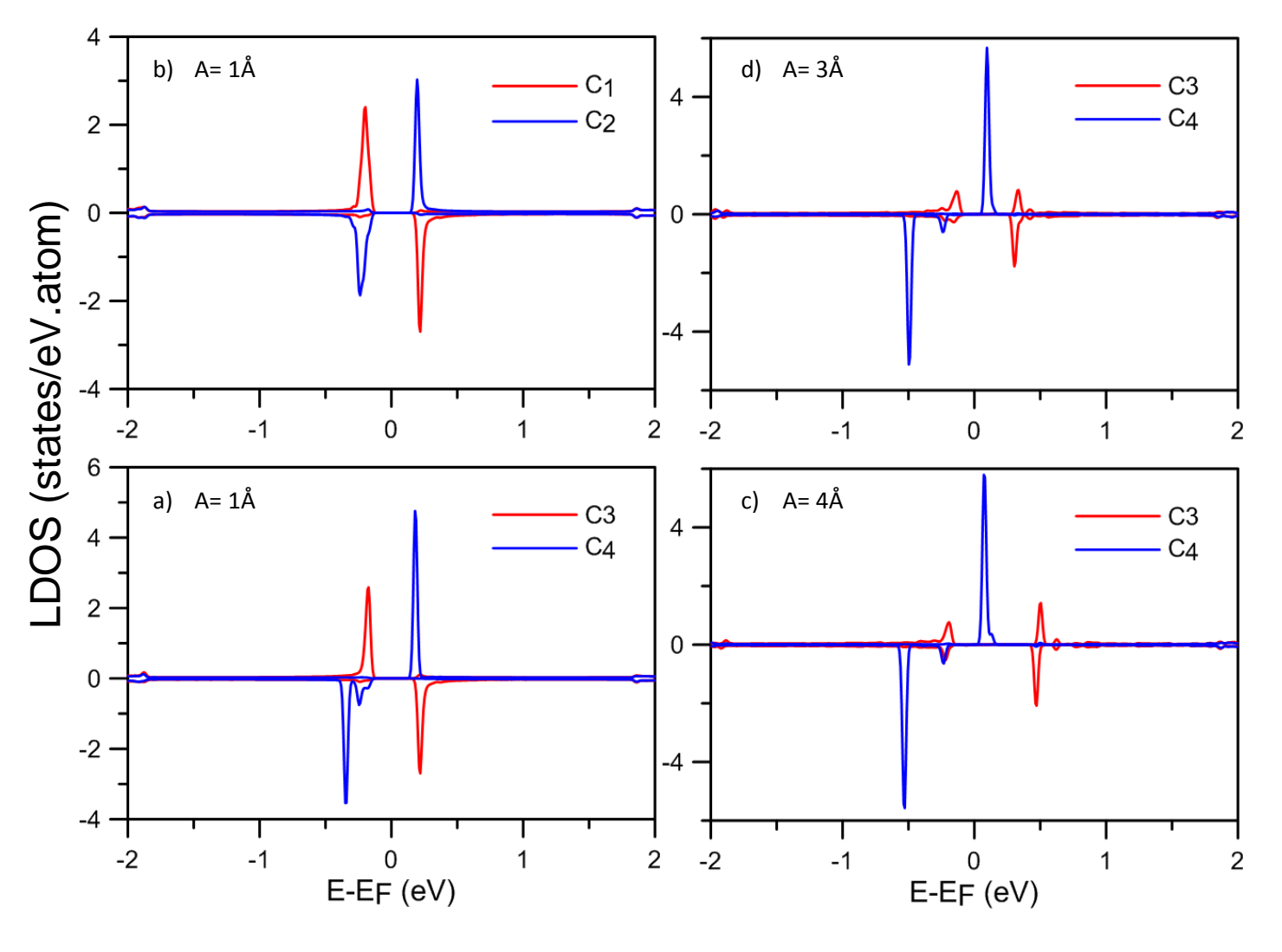


Figure 10